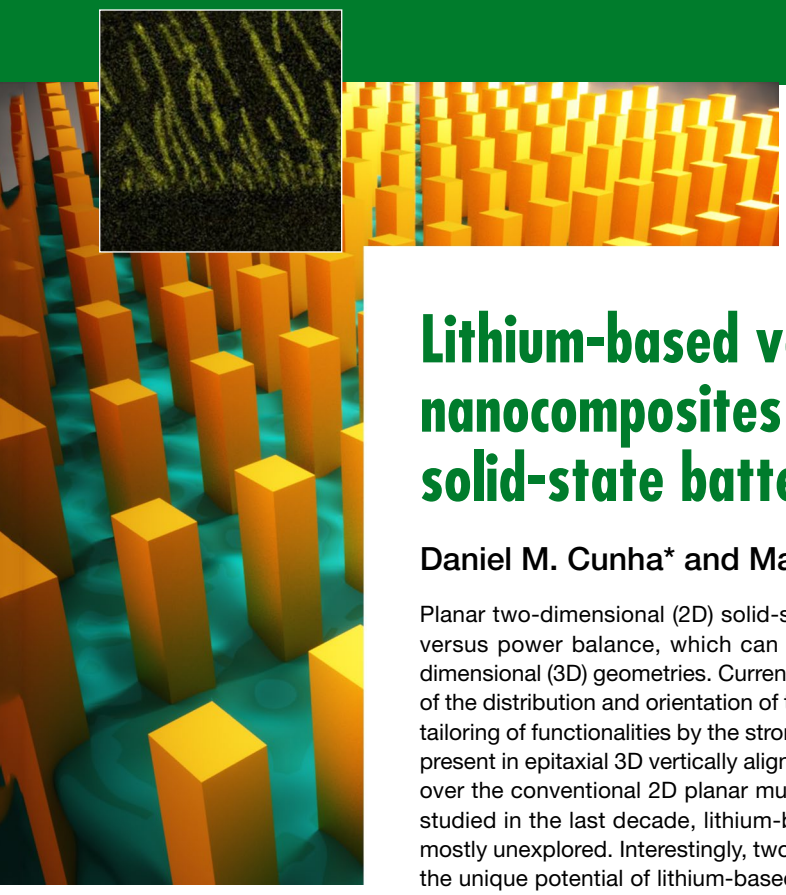

Lithium-based vertically aligned nanocomposites for three-dimensional solid-state batteries

Daniel M. Cunha* and Mark Huijben

Planar two-dimensional (2D) solid-state lithium-ion batteries exhibit an undesirable energy versus power balance, which can be dramatically improved by the application of three-dimensional (3D) geometries. Current ceramics-based nanocomposites exhibit limited control of the distribution and orientation of the nanoparticles within the matrix material. However, the tailoring of functionalities by the strong coupling between the two phases and their interfaces, present in epitaxial 3D vertically aligned nanocomposites (VANs), show promising advantages over the conventional 2D planar multilayers. Although a range of epitaxial VANs have been studied in the last decade, lithium-based VANs toward battery applications have remained mostly unexplored. Interestingly, two recent studies by Qi et al. and Cunha et al. demonstrate the unique potential of lithium-based VANs toward the realization of 3D solid-state batteries with enhanced energy storage performance. In this article, we will discuss these promising results as an enhanced current collector within the cathode or as an integrated solid-state cathode-electrolyte composite. Furthermore, we will describe different design configurations that can be applied to realize self-assembled VAN-based complete 3D battery devices.

Introduction

Since its introduction in 1991 by Sony, lithium-ion (Li-ion) batteries are the most popular rechargeable batteries,[1] as they have become the main power source for many applications, such as portable electronics, power tools, and hybrid/full electric vehicles. Tremendous research effort has been devoted to investigate the electrochemical performance of a wide variety of active lithium-based materials to develop batteries with large capacity, high energy and power density, improved safety, long cycle life, fast response, and low cost. Despite the efforts, none of the current rechargeable batteries can fully satisfy all of the challenging requirements for the projected energy storage needs. Key problems for this limitation include slow electrode process kinetics with high polarization and a low rate of ionic diffusion or electronic conductivity, particularly at the electrode–electrolyte interfaces.[2–4] The differences in ion-chemical potentials and Fermi levels at the interfaces lead to unwanted reactions, such as space charge layers and atomic intermixing, as well as parasitic side reactions and large structural rearrangements. Therefore, mastering control of the interfaces is identified as the grand challenge in energy storage research, being more important than designing new electrode and electrolyte materials. New research directions focused on interface structure optimization for ionic diffusion, electron transport, and the regulation of electrochemical reactions that are crucial for developing the urgently needed pathways to enhanced energy storage.

Current commercial lithium-ion batteries have an energy density of 300–500 mWh cm^{-3}, which is still far below the theoretical energy density of lithium-air batteries (2800 mWh cm^{-3}).[6] Common rechargeable batteries are based on organic liquid electrolytes, which result in several restrictions for their design and size due to the available separators and liquid electrolytes. Second, these acidic liquids cause unwanted reactions at the electrode surfaces, reducing the stability of the battery. Finally, these liquids carry the inherent risk of leakage and fire hazard. Therefore, the need for all solid-state microbatteries arises, which will exhibit enhanced safety, volumetric energy/power density, and chemical stability, see **Figure** 1.

One of the main issues with state-of-the-art solid-state electrolytes is the poor ionic conductivity compared to liquid organic electrolytes. Increasing the ionic conductivity of solid electrolytes is, therefore, an essential step to make further progress in this direction. However, while some promising solid electrolytes with lithium conductivities

Daniel M. Cunha, MESA+ Institute for Nanotechnology, University of Twente, The Netherlands; d.monteirocunha@utwente.nl
Mark Huijben, MESA+ Institute for Nanotechnology, University of Twente, The Netherlands; m.huijben@utwente.nl
*Corresponding author
doi:10.1557/s43577-021-00026-2

approaching those of liquid electrolytes have recently been reported for sulfide conductors (e.g., $Li_7P_3S_{11}$, $Li_{10}GeP_2S_{12}$, and $Li_{9.54}Si_{1.74}P_{1.44}S_{11.7}C_{l0.3}$),[7] stability issues limit the ionic transport across the electrode–electrolyte interface. In contrast, promising oxide electrolytes (e.g., perovskite $La_{0.5}Li_{0.5}TiO_3$, garnets $Li_7La_3Zr_2O_{12}$, LiPON ($Li_{2.88}PO_{3.73}N_{0.14}$), and LISICON ($Li_{14}ZnGe_4O_{16}$)),[7–9] with high chemical stabilities are currently limited by high grain-boundary resistances. Hence a dramatic reduction of the thickness of the solid electrolyte is required to overcome the limited lithium conductivity to enable fast charge–discharge rates.

Planar two-dimensional (2D) solid-state thin-film batteries exhibit an undesirable energy versus power balance, which can be dramatically improved by the application of three-dimensional (3D) geometries. An additional advantage of these 3D batteries is that the internal surface area between cathode, electrolyte, and anode is enlarged, improving their current output. This will ensure a giant step in power and energy density for solid-state devices, as depicted in Figure 1, allowing for a much better energy storage performance.[10–12] Several concepts for a 3D microbattery layout have been proposed in previous studies, based on membrane templates, interdigitated microrods, porous aerogels, microchannel plates, and anisotropic etching.[11,13,14] However, most of these designs are only conceptual, require multiple fabrication steps, or have only been focusing on partial solid-state devices. Furthermore, fabrication of such 3D batteries relies presently on the use of costly methods, such as microlithography and photolithography, or electrodeposition techniques combined with spin coating/infiltration. Therefore, the benefits of 3D batteries can only be fully exploited in the future if a synthetic route provides structure control of such systems down to the tens of nanometers length scales in combination with tunable crystal orientations of the individual materials and their shared interfaces.

The advantages of nanostructured materials are larger electrode/electrolyte contact area leading to higher (dis)charge rates, short path lengths for both electronic and Li-ion transport leading to higher charge flow, and better accommodation of the strain during lithium insertion/extraction. Various studies on Li-ion batteries have demonstrated that nanocrystalline intermetallic alloys, nanosized composite materials, carbon nanotubes, and nanosized transition-metal oxides are all promising new anode materials, while nanosized high-voltage cathodes $LiCoO_2$, $LiFePO_4$, and $LiMn_2O_4$ show higher capacity and better cycle life than their usual larger particle equivalents.[15]

Nanocomposites have attracted great interest over the last decades due to the presence of enhanced functional material properties induced by confinement of the structural dimensions.[16] Ceramics-based nanocomposites is a rapidly evolving research area,[17,18] as they are currently being used in a wide range of applications, such as motor engines, heat exchangers, power plants, and aircraft/spacecraft technology. However, accurate control of the distribution and orientation of the nanoparticles within the matrix material is often limited or impossible. Detailed knowledge on the alignment of nanostructures through self-assembly is well studied in organic systems,[19] and lately, more efforts are being done on inorganic, ceramic nanocomposites.

In parallel to 2D planar heterointerfaces, 3D vertical heteroepitaxial nanocomposite thin films have been developed in the past decade as a new materials' platform for creating self-assembled device architectures and multifunctionalities, as they show a wide range of attributes arising from the strong interplay among structural, electronic, magnetic, and even ionic properties.[20–23] Such epitaxial vertically aligned nanocomposites (VANs) offer promising advantages over conventional planar multilayers as key functionalities are tailored by the strong coupling between the two phases and their interfaces, such as strain-enhanced ferroelectricity and multiferroics,[24,25] enhanced ferromagnetism,[26] magnetoresistance,[27] electronic transport,[28] and coupled dielectric and optical effects.[29] Although a range of epitaxial VANs has been studied in the last decade,[22,23] lithium-based VANs toward battery applications have remained mostly unexplored. Interestingly, two recent studies by Qi et al.[30] and Cunha et al.[31] demonstrate the unique potential of lithium-based VANs toward the realization of 3D solid-state batteries with enhanced energy storage performance.

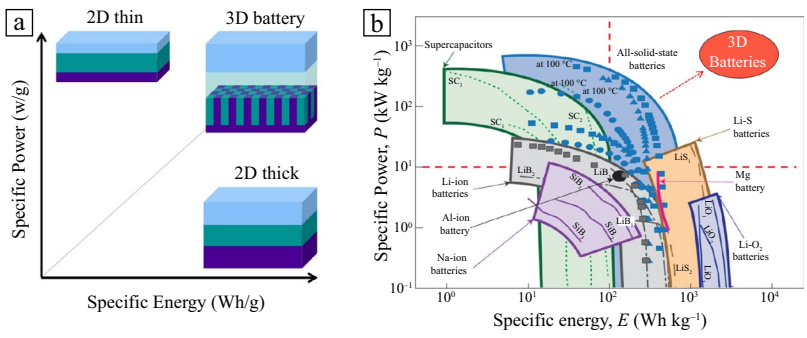

Figure 1. Ragone plots of (a) solid-state battery architectures illustrating the enhanced performance of a 3D nanocomposite system over a 2D planar film, (b) state-of-the-art lithium-ion battery technologies.[5]

Enhanced current collector within cathode

Cathode materials in Li-ion batteries are well-known for their limited electrical conductivity, which is the reason the carbon black is added to enhance the power density in conventional batteries. Recently, Qi et al.[30] demonstrated a new approach to improve the electrochemical performance of Li_2MnO_3 cathode thin films by introducing tilted Au nanopillars as effective current collectors. Due to its high theoretical capacity of 459 mAh g^{-1}, Li_2MnO_3 is a promising cathode material for high energy

density applications.[32,33] However, the low electrical conductivity of approximately 10^9 S cm^{-1} limits its power density. The approach by Qi et al. was the use of VAN-based thin-film electrodes to achieve higher electrical conductivity, as the proposed Li_2MnO_3–Au matrix-pillar configuration can provide more effective, continuous pathways for electrical and ionic transport across the entire cathode. Furthermore, the authors indicated that oxide–metal interfaces can provide better mechanical integrity and enhanced electrochemical cycling stability.

The metal Au nanopillars were incorporated into Li_2MnO_3 thin films through the oblique angle deposition (OAD) method[34] in pulsed laser deposition (PLD), as depicted in **Figure** 2a. The OAD technique was applied to facilitate the metal pillar formation and to avoid the agglomeration of metal particles in the oxide matrix.[35–38] The Li_2MnO_3–Au VAN film was deposited from a single target containing both materials on Al_2O_3 single crystalline substrates for structural analysis, as well as on stainless steel substrates buffered with Au for electrochemical measurements. The crystallographic analysis of the Li_2MnO_3/Au composite films by x-ray diffraction (XRD), shown in Figure 2b, indicates the highly textured growth of Li_2MnO_3 on both Al_2O_3 and Au stainless steel substrates, where the composite exhibits oriented Li_2MnO_3 (001) and Au (111) along the out-of-plane lattice direction.

The growth of the VAN film, exhibiting Au nanopillars embedded within Li_2MnO_3, was achieved and its formation on an Al_2O_3 substrate is shown in the energy dispersion x-ray (EDX) images in Figure 2c. Due to the set angle during OAD growth, the resulting Au nanopillars are tilted 19° from the out-of-plane direction, presenting an average diameter of ~6 nm and spacing of ~50 nm from each other. The *d*-spacings along the out-of-plane direction are measured to be 4.731 Å and 2.285 Å, corresponding to Li_2MnO_3(001) and Au(111).

The discontinuity observed in some of the Au pillars was attributed to the shadowing effect from the OAD growth. In this case, the small Au nanorods near the film–substrate interface are Au nucleates formed at the beginning stage of the growth that are shadowed by nearby taller pillars and stopped growing.[39] Furthermore, the discontinuity occurred along the nanopillars was credited to the different adatom diffusivity, generally lower in OAD growth.[40] Additionally, the tilting angle can be tuned by the PLD growth parameters.[41] Smaller tilt angle indicates slower growth rate, further indicating increased stability of in-plane growth and suppression of out-of-plane growth,[42] also reducing the shadowing effect.

The composite films on stainless steel were characterized electrochemically in coin cells using lithium metal disks (Sigma-Aldrich) as anode, Celgard 2400 PP (Celgard) as separator, and 1 M $LiPF_6$ salt dissolved in 1:1 volume ratio EC:DEC (Sigma-Aldrich) as electrolyte. The observed cycling behavior was enhanced as compared to pure Li_2MnO_3 thin-film cathodes, also prepared by PLD, and with thicknesses 6–20× thicker than previously reported studies.[43,44] Charge–discharge results show for the first cycle a total discharge capacity of 41.2 μAh cm^{-2} μm^{-1}, corresponding to 110.8 mAh g^{-1}, while a total capacity of 71.64 μAh cm^{-2} μm^{-1} (192.6 mAh g^{-1}) was observed for 100th cycle. The capacity increase of 74% was reported in the literature to be a result of a phase transformation upon cycling.[45] Cyclic voltammetry (CV) analysis was conducted to study the redox reactions in the nanocomposite thin-film electrode, see **Figure** 3a. Typical redox reactions for the spinel structure were observed, with intercalation of lithium-ion in the 16c octahedral and 8a tetrahedral sites for the redox pairs at 3 V and 4 V, respectively. Similar to the cycling test, the unexpected large anodic peak and the abnormal cathodic peak near 4 V confirm the existence of electrolyte decomposition.

Although the pure Li_2MnO_3 film failed after the 9th cycle, the Li_2MnO_3–Au composite film can be cycled for at least 100 cycles, with electrochemical performance improving with time, indicating that the proposed Au pillars increase the conductivity of the overall composite film. The enhanced current density within the VAN film was also demonstrated by the rate performance at different C-rates as shown in Figure 3b. The Li_2MnO_3–Au VAN film displayed good rate performance with 61% capacity retention at high rates of 14.8 C, corresponding to the current

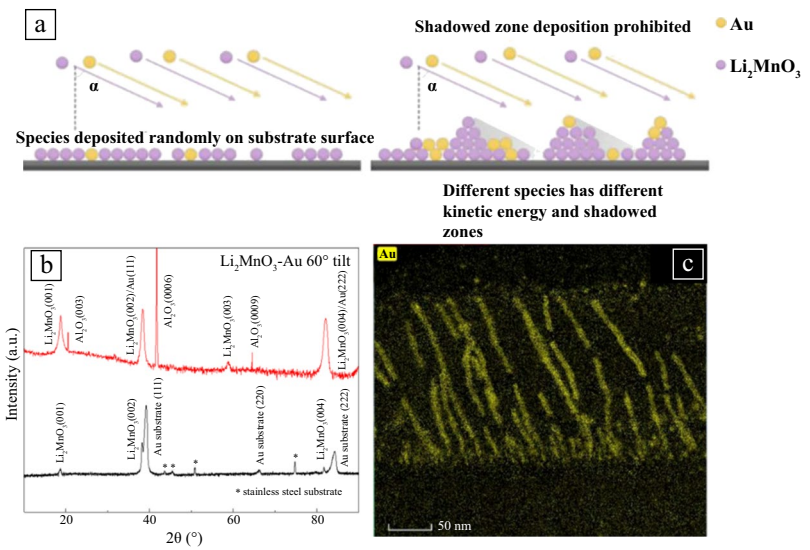

Figure 2. (a) Expected growth mechanism in oblique angle deposition by pulsed laser deposition. (b) Out-of-plane x-ray diffraction pattern of Li_2MnO_3–Au vertically aligned nanocomposite film on both Al_2O_3 and Au-buffered stainless steel substrates grown at 750°C and 0.067 mbar oxygen pressure. (c) Energy dispersion x-ray mapping for Au confirming the elemental distribution and the pillar formation.[30]

density of 80 μA cm^{-2}, as compared to slow rates of 0.57 C (5 μA cm^{-2}), which is higher than previously reported.[46,47] The battery analysis indicates an enhanced electrochemical performance of the promising Li_2MnO_3 cathode material due to the VAN structure with embedded Au-tilted nanopillars.

Integrated solid-state cathode–electrolyte

Many cathode materials exhibit limited Li-ion diffusivities, resulting in low power densities. This common behavior restricts their application for ultrafast charging and discharging performances. Reduction of the cathode material thickness will improve the power output as the Li-ions have to travel over a short distance, see Figure 1b. However, such thickness reduction consequently lowers the energy storage capacity at the same time due to the limited amount of Li-ions stored. A 3D architecture, combining a cathode with a solid-state electrolyte, would significantly reduce the pathway for Li-ions to travel within the cathode material together with the realization of the required cathode volume to store a large amount of Li-ions and, therefore, achieve a large energy capacity.

The incorporation of oriented cathode nanopillars into a solid electrolyte matrix was recently achieved via self-assembly in a single step VAN growth procedure.[31] The materials used were the spinel $LiMn_2O_4$ (LMO), a high-voltage cathode material[48] with a lattice parameter of $a = 8.245$ Å, and $La_{0.5}Li_{0.5}TiO_3$ (LLTO), a high ionic conducting electrolyte[49] with a perovskite structure ($a = 3.904$ Å), making them an interesting combination, similar to previous successful spinel-perovskite VAN formations.[24,50] The LMO-LLTO VAN films were grown by PLD on (100)-oriented Nb-doped (0.5 wt%) $SrTiO_3$ (Nb:STO) substrates from a sintered 67% $La_{0.5}Li_{0.5}TiO_3$ + 33% $LiMn_2O_4$ (30 wt% excess Li) target at a substrate temperature of 850°C, target–substrate distance of 5 cm, laser fluence of 2.3 J/cm^2, and frequency of 20 Hz, resulting in a growth rate of ~ 0.15 Å/pulse.

Following the trend of other perovskite-spinel systems reported (e.g., ordered pillars of $BaTiO_3$–$CoFe_2O_4$ and $BiFeO_3$–$CoFe_2O_4$),[24,50–53] the phase separation of both materials into a nanopillar-matrix structure within the nanocomposite was successfully achieved. The phase separation is shown by the scanning electron microscope (SEM) images, **Figure** 4a–b, and the XRD spectrum, in Figure 4c, which confirm the purity and crystallinity of both specific. The out-of-plane (100) crystal orientations of both LMO and LLTO phases within the VAN films are aligned with the (100) Nb:STO substrate orientation. In a good agreement with previous studies of individual LMO or LLTO thin films grown on crystalline STO(100), the LMO and LLTO peaks show the presence of highly crystalline-oriented spinel and perovskite structures.[54–56] The LLTO phase is epitaxially strained to the underlying STO substrate as determined by reciprocal space mapping XRD. The LLTO exhibits an out-of-plane lattice parameter of ~ 3.85 Å, which corresponds to a crystal structure with a volume equal to a relaxed cubic phase of about $Li_{0.3}La_{0.57}TiO_3$ with a lattice parameter of ~ 3.88 Å.[49] This indicates a 0.06% in-plane strain in the LLTO unit cell. The LMO phase is not strained to the underlying STO substrate, but relaxed to a cubic spinel structure with a lattice parameter of 8.42 Å. The extra peaks with lower intensity indicate the presence of minor contributions of the tetragonal LLTO ($Li_{0.56}La_{0.33}TiO_3$), which could be embedded in the LLTO matrix or located at specific interfaces. The in-plane orientations of both cubic LMO and LLTO phases are aligned to the cubic substrate as confirmed by detailed XRD analysis resulting in square LMO nanopillars rotated 45° with respect to the (010) in-plane direction of both the perovskite LLTO matrix and STO substrate. Additionally, Figure 4d shows the phase separation by energy selective backscattered (ESB) SEM analysis, where contrast is determined by compositional differences, resulting in a brighter LLTO matrix due to the presence of heavy La ions.

The study focused on how different growth parameters, such as temperature and deposition rate, can influence the size and distribution of the nanopillars over the surface.[31] In order to analyze this relation, a Kinetic Monte Carlo (KMC) model to simulate the nanopillar formation was used. In contrast with the KMC models presented previously in the literature, the proposed model introduced higher degrees of freedom and activation energies for hopping obtained experimentally via reflective high energy electron diffraction (RHEED) measurements.[31]

Kinetic Monte Carlo simulations (KMCS) for the VAN surface after 300 pulses of the nanocomposite growth at different temperatures is shown in **Figure** 5. The two components phase separate into well-defined and evenly spaced nanostructures, and the trends observed are in good agreement with the VANs obtained experimentally, shown by the atomic force microscope images. Although the growth

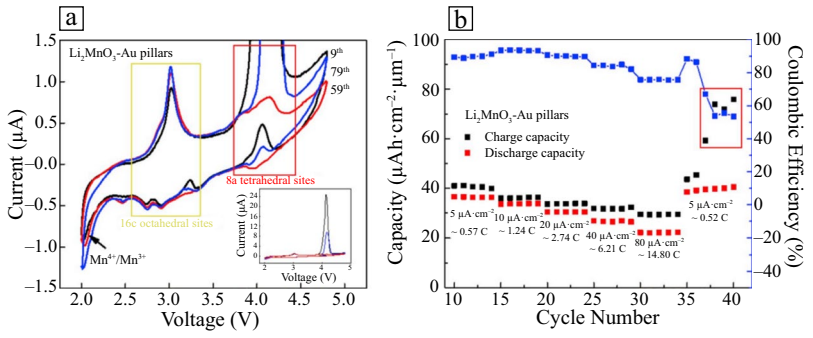

Figure 3. (a) Cyclic voltammograms of Li_2MnO_3–Au vertically aligned nanocomposite film with potential 20 μV s^{-1} sweep rate at 9th, 59th, and 79th cycle. (b) C-rate performance test at different current densities.[30]

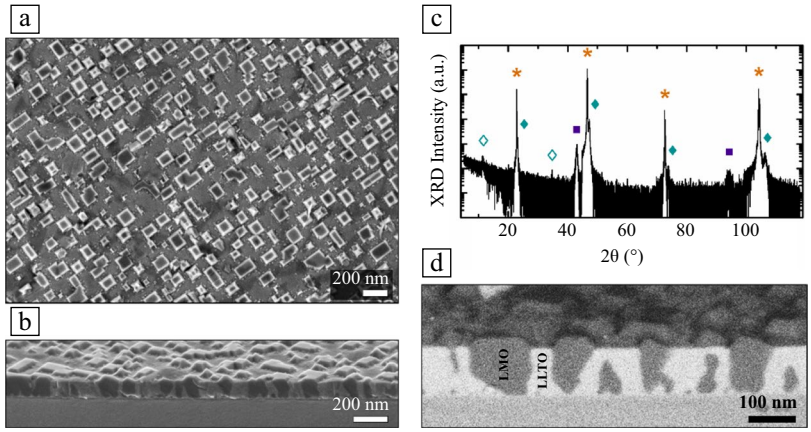

Figure 4. (a) Top-view and (b) cross-sectional scanning electron microscope (SEM) images of a nanocomposite thin film composed of $LiMn_2O_4$ (LMO) pillars embedded in $La_{0.5}Li_{0.5}TiO_3$ (LLTO) matrix. (c) X-ray diffraction (XRD) analysis of the vertically aligned nanocomposite film, in which LLTO peaks are shown by ★, LMO by ◆, and the $SrTiO_3$ substrate peaks by ■, whereas minor contributions of the tetragonal LLTO phase are indicated by ◊. (d) Cross-sectional energy selective backscattered SEM image showing the compositional contrast.[31]

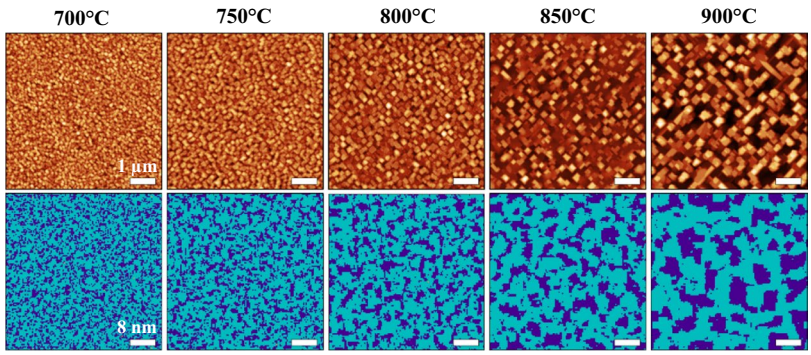

Figure 5. Atomic force microscope images (top) and Kinetic Monte Carlo simulations results (bottom) for the $LiMn_2O_4$–$Li_{0.5}La_{0.5}TiO_3$ nanocomposite growth at a deposition rate of 20 Hz for different growth temperatures.[31]

temperature is a key factor that affects the nanopillar shape,[57] as the shape of the nanopillars is determined by the competition between the strain energy and interfacial energy,[58] the KMCS model does not incorporate anisotropic interaction energies to reflect different crystal facets and disregards the thermodynamic processes for energy reduction at the interfaces between the different material phases (i.e., nanopillar and matrix).

Because the interaction energies are relatively close, the LMO and LLTO components show some intermixing. Increasing the difference between these values would lead to stronger phase separation.[59] Nevertheless, the simulated vertical nanostructures are qualitatively similar to those described in other simulated nanocomposite studies.[59–63] A quantitative analysis was also performed considering the number density of pillars over the VAN surface. The number density comparison between KMCS and experimental results as a function of the different substrate temperatures for a 20 Hz deposition rate, and the different deposition rates for a substrate temperature of 800°C, is shown by **Figure** 6a–b, respectively. The KMCS results show good agreement with the evolution of pillar density upon changes in synthesis parameters, with a difference of a factor of 100. This difference is caused by the static contribution (E_S) values used in the KMCS. E_S is the surface energy, or the activation energy for hopping of a free adatom. The term was introduced by Ratsch et al.,[64] and in the model sets the number of hops per pulse. A lower E_S value increases the number of hops per pulse, which, in turn, results in an increase of the computational time of the simulation. For the results presented, $E_S = 1.0$ eV was used, which generates qualitatively good results for a low computational cost. Extrapolating KMCS number densities for different E_S values from Figure 6b to the experimental number density of 7.6×10^{-5} nm^{-2} for a 50 Hz deposition rate, an E_S value of 0.38 eV is calculated, resulting in an estimated increase of computational time for the KMC simulation of two orders of magnitude. The study demonstrates the promising capability to combine state-of-the-art cathode and solid-state electrolyte materials into a highly ordered VAN structure enabling further optimization of the electrochemical performance.

Conclusion

Although various epitaxial VANs have been studied in the last decade, exploration of lithium-based VANs for enhanced energy storage has only started recently. The first studies show promising results as an enhanced current collector within the cathode[30] or as an integrated solid-state cathode-electrolyte composite.[31] However, more fundamental understanding about the diffusion of Li-ions in such epitaxial VAN structures is required during intercalation across the vertical epitaxial interfaces within the electrodes (cathodes and anodes) or toward the adjacent electrolyte.

For the development of complete 3D battery devices, several different design configurations can be applied with increasing complexity, see **Figure** 7. Current solid-state battery devices are based on 2D planar architectures with the limitations in

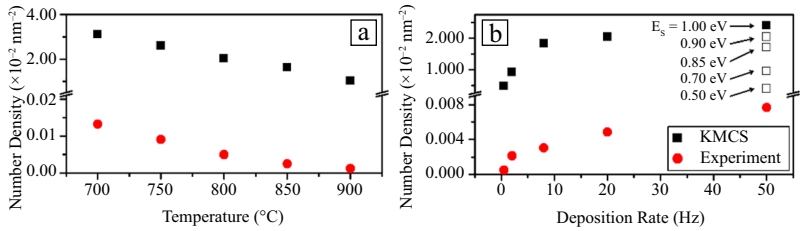

Figure 6. Number density comparison between Kinetic Monte Carlo simulations (■) and experimental results (●) as a function of (a) different substrate temperatures for a 20 Hz deposition rate and (b) different deposition rates for a substrate temperature of 800°C. White squares (□) in (b) represent different E_S values used during simulations.[31]

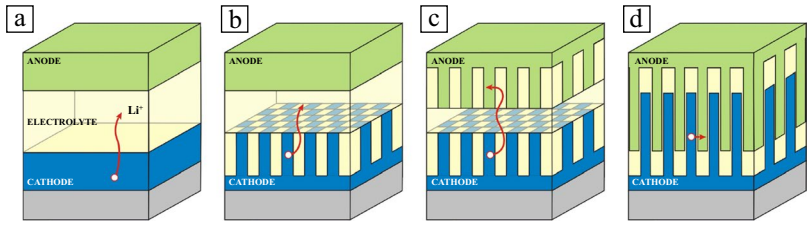

Figure 7. Epitaxial vertically aligned nanocomposite-based solid-state battery configurations: (a) 2D planar, (b) 2D/3D-combined, (c) partial 3D-integrated, and (d) full 3D-interdigitated solid-state batteries. Example of lithium-ion pathway is indicated by the red arrow.

energy versus power optimization, as discussed in the introduction. Introduction of a 3D-based electrode (e.g., cathode) will require an additional electrolyte layer before applying the final 2D anode layer to create a 2D/3D-combined configuration. However, the 2D anode layer could also be replaced by a 3D-based anode layer to realize a partial 3D-integrated configuration. Preliminary experiments in our laboratory have shown promising results for combinations between the spinel $LiMn_2O_4$ (cathode),[54] spinel $Li_4Ti_5O_{12}$ (anode),[65] and perovskite $La_{0.5}Li_{0.5}TiO_3$ (electrolyte),[31] although many more oxide lithium-based materials are available to explore. Finally, the synthesis of a full 3D-interdigitated battery configuration would require the self-assembly of a three-component 3D nanocomposite at the center of the battery device. Such self-assembled three-component vertically aligned nanocomposite has not been realized yet and will require a very subtle balance of the interaction energies between all involved materials. This configuration would exhibit the highest complexity with the sequential deposition of three specific layers on top of each other: first a two-phase cathode/electrolyte layer, second a three-phase cathode/electrolyte/anode layer, and finally a two-phase anode/electrolyte layer to realize a complete device.

The crystal structure of the electrode nanopillars, electrolyte matrix, and their interfaces will determine the lithium diffusion mechanism within the complete structure, which will eventually be crucial for the battery performance. Therefore, variations to the size and orientations of the crystal structures within all components will need to be studied to characterize the relationship between them. The dependence of the energy storage behavior in complete solid-state battery devices on the specific formation of epitaxial VANs of various cathode/electrolyte/anode nanocomposites will need to be studied regarding the size distribution of the nanopillar-matrix structures and the crystal orientations at the incorporated interfaces. The energy storage performance should be explored by using standard battery testing techniques, such as galvanostatic cycling, cyclic voltammetry, rate capability experiments, potentiostatic intermittent titration technique, and electrochemical impedance spectroscopy, to determine the dependence of the energy storage content, power output, rate of charge, and cycle life performance on the structure and composition of the nanocomposites. However, recent development *in operando* characterization techniques will enable monitoring of the lithium intercalation mechanisms at the length scales of the nanopillar-matrix structures, with a focus on the detailed ionic transport across the epitaxial interfaces.

Acknowledgments

D.M.C. and M.H. acknowledge support from The Netherlands Organization for Scientific Research (NWO) under VIDI Grant No. 13456.

Conflict of interest

On behalf of all authors, the corresponding author states that there is no conflict of interest.

Open Access

References

1. M. Li, J. Lu, Z. Chen, K. Amine, *Adv. Mater.* **30**, 1 (2018)
2. A.C. Luntz, J. Voss, K. Reuter, *J. Phys. Chem. Lett.* **6**, 4599 (2015)
3. K.X. Wang, X.H. Li, J.S. Chen, *Adv. Mater.* **27**, 527 (2015)
4. Y. Yuan, K. Amine, J. Lu, R. Shahbazian-Yassar, *Nat. Commun.* **8**, 1 (2017)
5. Y. Kato, S. Hori, T. Saito, K. Suzuki, M. Hirayama, A. Mitsui, M. Yonemura, H. Iba, R. Kanno, *Nat. Energy* **1**, 1 (2016)
6. N. Nitta, F. Wu, J.T. Lee, G. Yushin, *Mater. Today* **18**, 252 (2015)
7. A. Manthiram, X. Yu, S. Wang, *Nat. Rev. Mater.* **2**, 1 (2017)
8. K.K. Bharathi, H. Tan, S. Takeuchi, L. Meshi, H. Shen, J. Shin, I. Takeuchi, L.A. Bendersky, *RSC Adv.* **6**, 61974 (2016)
9. K.H. Kim, Y. Iriyama, K. Yamamoto, S. Kumazaki, T. Asaka, K. Tanabe, C.A.J. Fisher, T. Hirayama, R. Murugan, Z. Ogumi, *J. Power Sources* **196**, 764 (2011)
10. J.W. Long, B. Dunn, D.R. Rolison, H.S. White, *Chem. Rev.* **104**, 4463 (2004)
11. J.F.M. Oudenhoven, L. Baggetto, P.H.L. Notten, *Adv. Energy Mater.* **1**, 10 (2011)
12. C. Yue, J. Li, L. Lin, *Front. Mech. Eng.* **12**, 459 (2017)
13. S. Ferrari, M. Loveridge, S.D. Beattie, M. Jahn, R.J. Dashwood, R. Bhagat, *J. Power Sources* **286**, 25 (2015)
14. T.S. Arthur, D.J. Bates, N. Cirigliano, D.C. Johnson, P. Malati, J.M. Mosby, E. Perre, M.T. Rawls, A.L. Prieto, B. Dunn, *MRS Bull.* **36**, 523 (2011)
15. P.G. Bruce, B. Scrosati, J.-M. Tarascon, *Angew. Chem. Int. Ed.* **47**, 2930 (2008)
16. E.T. Thostenson, C. Li, T.W. Chou, *Compos. Sci. Technol.* **65**, 491 (2005)
17. P. Palmero, *Nanomaterials* **5**, 656 (2015)
18. X. Sun, J. Huang, J. Jian, M. Fan, H. Wang, Q. Li, J.L. MacManus-Driscoll, P. Lu, X. Zhang, H. Wang, *Mater. Horiz.* **5**, 536 (2018)
19. M.A.C. Stuart, W.T.S. Huck, J. Genzer, M. Müller, C. Ober, M. Stamm, G.B. Sukhorukov, I. Szleifer, V.V. Tsukruk, M. Urban, F. Winnik, S. Zauscher, I. Luzinov, S. Minko, *Nat. Mater.* **9**, 101 (2010)
20. M. Imada, A. Fujimori, Y. Tokura, *Rev. Mod. Phys.* **70**, 1039 (1998)
21. D. Elbio, *Science* **309**, 257 (2005)
22. W. Zhang, R. Ramesh, J.L. MacManus-Driscoll, H. Wang, *MRS Bull.* **40**, 736 (2015)
23. J. Huang, J.L. MacManus-Driscoll, H. Wang, *J. Mater. Res.* **32**, 4054 (2017)
24. H. Zheng, J. Wang, S.E. Lofland, Z. Ma, L. Mohaddes-Ardabili, T. Zhao, L. Salamanca-Riba, S.R. Shinde, S.B. Ogale, F. Bai, D. Viehland, Y. Jia, D.G. Schlom, M. Wuttig, A. Roytburd, R. Ramesh, *Science* **303**, 661 (2004)
25. S.A. Harrington, J. Zhai, S. Denev, V. Gopalan, H. Wang, Z. Bi, S.A.T. Redfern, S.H. Baek, C.W. Bark, C.B. Eom, Q. Jia, M.E. Vickers, J.L. MacManus-Driscoll, *Nat. Nanotechnol.* **6**, 491 (2011)
26. Z. Wang, Y. Li, R. Viswan, B. Hu, V.G. Harris, J. Li, D. Viehland, *ACS Nano* **7**, 3447 (2013)
27. A. Chen, Z. Bi, C.F. Tsai, J. Lee, Q. Su, X. Zhang, Q. Jia, J.L. MacManus-Driscoll, H. Wang, *Adv. Funct. Mater.* **21**, 2423 (2011)
28. Y.H. Hsieh, J.M. Liou, B.C. Huang, C.W. Liang, Q. He, Q. Zhan, Y.P. Chiu, Y.C. Chen, Y.H. Chu, *Adv. Mater.* **24**, 4564 (2012)
29. O. Lee, S.A. Harrington, A. Kursumovic, E. Defay, H. Wang, Z. Bi, C.F. Tsai, L. Yan, Q. Jia, J.L. MacManus-Driscoll, *Nano Lett.* **12**, 4311 (2012)
30. Z. Qi, J. Tang, S. Misra, C. Fan, P. Lu, J. Jian, Z. He, V.G. Pol, X. Zhang, H. Wang, *Nano Energy* **69**, 104381 (2020)
31. D.M. Cunha, C.M. Vos, T.A. Hendriks, D.P. Singh, M. Huijben, *ACS Appl. Mater. Interfaces* **11**, 44444 (2019)
32. A.D. Robertson, P.G. Bruce, *Chem. Commun.* **2002**(23), 2790 (2002)
33. S.F. Amalraj, D. Sharon, M. Talianker, C.M. Julien, L. Burlaka, R. Lavi, E. Zhecheva, B. Markovsky, E. Zinigrad, D. Kovacheva, R. Stoyanova, D. Aurbach, *Electrochim. Acta* **97**, 259 (2013)
34. A. Barranco, A. Borras, A.R. Gonzalez-Elipe, A. Palmero, *Prog. Mater. Sci.* **76**, 59 (2016)
35. Z. Qi, J. Jian, J. Huang, J. Tang, H. Wang, V.G. Pol, H. Wang, *Nano Energy* **46**, 290 (2018)
36. M. Lambert, A. May, C.K. Akkan, N. Agarwal, O.C. Aktas, *Mater. Lett.* **137**, 405 (2014)
37. S. Misra, L. Li, D. Zhang, J. Jian, Z. Qi, M. Fan, H.-T. Chen, X. Zhang, H. Wang, *Adv. Mater.* **31**, 1806529 (2019)
38. J. Jian, X. Wang, S. Misra, X. Sun, Z. Qi, X. Gao, J. Sun, A. Donohue, D.G. Lin, V. Pol, J. Youngblood, H. Wang, L. Li, J. Huang, H. Wang, *Adv. Funct. Mater.* **29**, 1903690 (2019)
39. Y. He, J. Fu, Y. Zhao, *Front. Phys.* **9**, 47 (2014)
40. Y. He, Y. Zhao, *Nanoscale* **3**, 2361 (2011)
41. A. Chen, Z. Bi, C.-F. Tsai, L. Chen, Q. Su, X. Zhang, H. Wang, *Cryst. Growth Des.* **11**, 5405 (2011)
42. B.H. Stafford, M. Sieger, R. Ottolinger, A. Meledin, N.M. Strickland, S.C. Wimbush, G. Van Tendeloo, R. Hühne, L. Schultz, *Supercond. Sci.* Technol. **30**, 55002 (2017)
43. S. Taminato, M. Hirayama, K. Suzuki, N.L. Yamada, M. Yonemura, J.Y. Son, R. Kanno, *Chem. Commun.* **51**, 1673 (2015)
44. K. Hikima, K. Suzuki, S. Taminato, M. Hirayama, S. Yasuno, R. Kanno, *Chem. Lett.* **48**, 192 (2019)
45. V.K. Vendra, T.Q. Nguyen, A.K. Thapa, J.B. Jasinski, M.K. Sunkara, *RSC Adv.* **5**, 36906 (2015)
46. H. He, H. Cong, Y. Sun, L. Zan, Y. Zhang, *Nano Res.* **10**, 556 (2017)
47. L. Xiong, M. Sun, Y. Xu, X. Du, X. Xiao, *Solid State Ionics* **325**, 170 (2018)
48. M.M. Thackeray, *Prog. Solid State Chem.* **25**, 1 (1997)
49. S. Stramare, V. Thangadurai, W. Weppner, *Chem. Mater.* **34**, 3974 (2003)
50. H. Zheng, F. Straub, Q. Zhan, P.L. Yang, W.K. Hsieh, F. Zavaliche, Y.H. Chu, U. Dahmen, R. Ramesh, *Adv. Mater.* **18**, 2747 (2006)
51. C. Schmitz-Antoniak, D. Schmitz, P. Borisov, F.M.F. de Groot, S. Stienen, A. Warland, B. Krumme, R. Feyerherm, E. Dudzik, W. Kleemann, H. Wende, *Nat. Commun.* **4**, 2051 (2013)
52. A. Chen, Y. Dai, A. Eshghinejad, Z. Liu, Z. Wang, J. Bowlan, E. Knall, L. Civale, J.L. MacManus-Driscoll, A.J. Taylor, R.P. Prasankumar, T. Lookman, J. Li, D. Yarotski, Q. Jia, *Adv. Sci.* **6**, 1901000 (2019)
53. H. Zheng, Q. Zhan, F. Zavaliche, M. Sherburne, F. Straub, M.P. Cruz, L.-Q. Chen, U. Dahmen, R. Ramesh, *Nano Lett.* **6**, 1401 (2006)
54. R. Hendriks, D.M. Cunha, D.P. Singh, M. Huijben, *ACS Appl. Energy Mater.* **1**, 7046 (2018)
55. H. Ohta, T. Mizoguchi, N. Aoki, T. Yamamoto, A. Sabarudin, T. Umemura, *Appl. Phys. Lett.* **100**, 173107 (2012)
56. X. Chen, M. Vörös, J.C. Garcia, T.T. Fister, D.B. Buchholz, J. Franklin, Y. Du, T.C. Droubay, Z. Feng, H. Iddir, L.A. Curtiss, M.J. Bedzyk, P. Fenter, *ACS Appl. Energy Mater.* **1**, 2526 (2018)
57. L. Mohaddes-Ardabili, H. Zheng, S.B. Ogale, B. Hannoyer, W. Tian, J. Wang, S.E. Lofland, S.R. Shinde, T. Zhao, Y. Jia, L. Salamanca-Riba, D.G. Schlom, M. Wuttig, R. Ramesh, *Nat. Mater.* **3**, 533 (2004)
58. A. Chen, Q. Su, H. Han, E. Enriquez, Q. Jia, *Adv. Mater.* **31**, 1803241 (2019)
59. S. Zheng, W. Zhu, Y.F. Gao, G.M. Stocks, Z. Zhang, *Appl. Phys. Lett.* **96**, 071913 (2010)
60. J.C. Walter, G.T. Barkema, *Phys. A Stat. Mech. Appl.* **418**, 78 (2015)
61. I. Mouton, E. Talbot, C. Pareige, R. Lardé, D. Blavette, *J. Appl. Phys.* **115**, 053515 (2014)
62. Y. Ichino, A. Tsuruta, S. Miura, Y. Yoshida, M. Yoshizumi, T. Izumi, *IEEE Trans. Appl. Supercond.* **25**, 6995944 (2015)
63. P.M. Lam, S.J. Liu, C.H. Woo, *Phys. Rev. B Condens. Matter Mater. Phys.* **66**, 454081 (2002)
64. C. Ratsch, A. Zangwill, P. Smilauer, D.D. Vvedensky, *Phys. Rev. Lett.* **72**, 3194 (1994)
65. D.M. Cunha, T.A. Hendriks, A. Vasileiadis, C.M. Vos, T. Verhallen, D.P. Singh, M. Wagemaker, M. Huijben, *ACS Appl. Energy Mater.* **2**, 3410 (2019) □

Daniel M. Cunha is a researcher at the University of Twente, The Netherlands, on the study of different aspects of thin-film solid-state batteries. He received his energy engineering degree from the Federal University of ABC, Santo André, Brazil, in 2015, where he also conducted research projects in condensed matter physics and nanoscience for energy applications. He received his PhD degree in self-assembled vertically aligned nanocomposites for solid-state batteries from the Inorganic Materials Science Group at the University of Twente. Cunha can be reached by email at d.monteirocunha@utwente.nl.

Mark Huijben is a professor of nanomaterials for energy conversion and storage at the MESA+ Institute for Nanotechnology of the University of Twente, The Netherlands. He received his PhD degree in 2006 from the University of Twente. He completed postdoctoral research on interfaces in complex oxides at the University of California, Berkeley. In 2009, he started his research group at the University of Twente, which he has combined since 2018 with a guest scientist position at Forschungszentrum Jülich. His research focuses on novel nanostructured thin films with advanced structural and functional properties at the incorporated interfaces. The aim is to develop new materials toward improved energy applications, such as solid-state batteries and thermoelectric energy generators. Huijben can be reached by email at m.huijben@utwente.nl.